Fiber-optic confocal microscope using a MEMS scanner and miniature objective lens

Hyun-Joon Shin[1,2], Mark C. Pierce[1], Daesung Lee[3], Hyejun Ra[3], Olav Solgaard[3], and Rebecca Richards-Kortum[1*]

[1]*Department of Bioengineering, Rice University, Houston, TX 77251, USA*
[2]*Korea Institute of Science and Technology, Seoul 136-791, Republic of Korea*
[3]*Department of Electrical Engineering, Stanford University, Stanford, CA 94305, USA*
[*] *rkortum@rice.edu*

Abstract: We designed and constructed a single-fiber-optic confocal microscope (SFCM) with a microelectromechanical system (MEMS) scanner and a miniature objective lens. Axial and lateral resolution values for the system were experimentally measured to be 9.55 μm and 0.83 μm respectively, in good agreement with theoretical predictions. Reflectance images were acquired at a rate of 8 frames per second, over a 140 μm x 70 μm field-of-view. In anticipation of future applications in oral cancer detection, we imaged *ex vivo* and *in vivo* human oral tissue with the SFCM, demonstrating the ability of the system to resolve cellular detail.

OCIS codes: (170.1790) Medical optics and biotechnology: Confocal microscopy; (170.4580) Medical optics and biotechnology: Optical diagnostics for medicine

References and Links

1. J. B. Pawley, ed. *Handbook of confocal microsopy*, 2nd edn. (Plenum, New York, 1995).
2. M. Rajadhyaksha, R. R. Anderson, and R. H. Webb, "Video-rate confocal scanning laser microscope for imaging human tissues *in vivo*," Appl. Opt. **38**, 2105-2115 (1999).
3. R. H. Webb, G. W. Hughes, and F. C. Delori, "Confocal scanning laser ophthalmoscope," Appl. Opt. **26**, 1492-1499 (1987).
4. K. C. New, W. M. Petroll, A. Boyde, L. Martin, P. Corcuff, J. L. Leveque, M. A. Lemp, H. D. Cavanagh, and J. V. Jester, "*In vivo* imaging of human teeth and skin using real-time confocal microscopy," Scanning **13**, 369-372 (1991).
5. K. D. Carlson, "Fiber optic confocal microscope: *in vivo* precancer detection", PhD thesis, The University of Texas at Austin, 2006.
6. K. B. Sung, R. Richards-Kortum, M. Follen, A. Malpica, C. Liang, and M. Descour, "Fiber optic confocal reflectance microscopy: a new real-time technique to view nuclear morphology in cervical squamous epithelium *in vivo*," Opt. Express **11**, 3171-3181 (2003).
7. M. R. Harris, "Scanning microscope with a miniature head," U.K. patent GB 2 340 332 B (2001).
8. A. L. Polglase, W. McLaren, S. Skinner, R. Kiesslich, M. Neurath, and P. Delaney, "A fluorescence confocal endomicroscope for *in vivo* microscopy of the upper- and lower-GI tract," Gastrointest. Endosc. **62**, 686-695 (2005).
9. E. J. Seibel and Q. Y. J. Smithwick, "Unique features of optical scanning, single fiber endoscopy," Lasers Surg. Med. **30**, 177-183 (2002).
10. L. Giniunas, R. Juskaitis, and S. V. Shatalin, "Scanning fiber-optic microscope," Electron. Lett. **27**, 724-726 (1991).
11. C. Boudoux, S. H. Yun, W. Y. Oh, W. M. White, N. V. Iftimia, M. Shishkov, B. E. Bouma, and G. J. Tearney, "Rapid wavelength-swept spectrally encoded confocal microscopy," Opt. Express **13**, 8214-8221 (2005).
12. D. Yelin, C. Boudoux, B. E. Bouma, and G. J. Tearney, "Large area confocal microscopy," Opt. Lett. **32**, 1102-1104 (2007).
13. A. F. Gmitro and D. Aziz, "Confocal microscopy through a fiber-optic imaging bundle," Opt. Lett. **18**, 565-567 (1993).
14. E. Laemmel, M. Genet, G. Le Goualher, A. Perchant, J-F. Le Gargasson, and E. Vicaut, "Fibered confocal fluorescence microscopy (Cell-viZio™) facilitates extended imaging in the field of microcirculation," J. Vasc. Res. **41**, 400-411 (2004).

#82105 - $15.00 USD Received 16 Apr 2007; revised 7 Jun 2007; accepted 8 Jun 2007; published 10 Jul 2007

15. P. M. Lane, A. L. P. Dlugan, R. Richards-Kortum, and C. E. MacAulay, "Fiber-optic confocal microscopy using a spatial light modulator," Opt. Lett. **25**, 1780-1782 (2000).
16. Y. S. Sabharwal, A. R. Rouse, L. Donaldson, M. F. Hopkins, and A. F. Gmitro "Slit-scanning confocal microendoscope for high-resolution *in vivo* imaging," Appl. Opt. **38**, 7133-7144 (1999).
17. A. R. Rouse, A. Kano, J. A. Udovich, S. M. Kroto, and A. F. Gmitro, "Design and demonstration of a miniature catheter for a confocal microendoscope," Appl. Opt. **43**, 5763-5771 (2004).
18. H. Miyajima, K. Murakami, and M. Katashiro, "MEMS Optical Scanners for Microscopes," IEEE J. Sel. Top. Quantum. Electron. **10**, 514-527 (2004).
19. D. L. Dickensheets and G. S. Kino, "Micromachined scanning confocal optical microscope," Opt. Lett. **21**, 764-766 (1996).
20. S. Kwon and L. P. Lee, "Micromachined transmissive scanning confocal microscope," Opt. Lett. **29**, 706-708 (2004).
21. K. C. Maitland, H. J. Shin, H. Ra, D. Lee, O. Solgaard, and R. Richards-Kortum, "Single fiber confocal microscope with a two-axis gimbaled MEMS scanner for cellular imaging," Opt. Express **14**, 8604-8612 (2006).
22. J. T. C. Liu, M. J. Mandella, H. Ra, L. K. Wong, O. Solgaard, G. S. Kino, W. Piyawattanametha, C. H. Contag, and T. D. Wang, "Miniature near-infrared dual-axes confocal microscope utilizing a two-dimensional microelectromechanical systems scanner," Opt. Lett. **32**, 256-258 (2007).
23. B. A. Flusberg, E. D. Cocker, W. Piyawattanametha, J. C. Jung, E. L. M. Cheung, and M. J. Schnitzer, "Fiber-optic fluorescence imaging," Nat. Methods **2**, 941-950 (2005).
24. C. Liang, K. B. Sung, R. Richards-Kortum, and M. Descour, "Design of a high-numerical-aperture miniature microscope objective for an endoscopic fiber confocal microscope," Appl. Opt. **41**, 4603-4610 (2002).
25. R. T. Kester, T. S. Tkaczyk, M. R. Descour, T. Christenson, and R. Richards-Kortum, "High numerical aperture microendoscope objective for a fiber confocal reflectance microscope," Opt. Express **15**, 2409-2420 (2007).
26. W. Jung, D. T. McCormick, J. Zhang, L. Wang, N. C. Tien, and Z. Chen, "Three-dimensional endoscopic optical coherence tomography by use of a two-axis microelectromechanical scanning mirror," Appl. Phys. Lett. **88**, 163901 (2006).
27. J. J. Bernstein, T. W. Lee, F. J. Rogomentich, M. G. Bancu, K. H. Kim, G. Maguluri, B. E. Bouma, and J. F. de Boer, "Scanning OCT endoscope with 2-axis magnetic micromirror," Proc. SPIE **6432**, 64320L (2007).
28. W. Piyawattanametha, R. P. J. Barretto, T. H. Ko, B. A. Flusberg, E. D. Cocker, H. Ra, D. Lee, O. Solgaard, and M. J. Schnitzer, "Fast-scanning two-photon fluorescence imaging based on a microelectromechanical systems two-dimensional scanning mirror," Opt. Lett. **31**, 2018-2020 (2006).
29. D. Lee and O. Solgaard. "Two-axis gimbaled microscanner in double SOI layers actuated by self-aligned vertical electrostatic combdrive," in *Proceedings of the Solid-State Sensors, Actuators and Microsystems Workshop*, Hilton Head Island, (2004), pp. 352-355.
30. H. Ra, W. Piyawattanametha, Y. Taguchi, and O. Solgaard, "Dual-axes confocal fluorescence microscopy with a two-dimensional MEMS scanner," Proc. IEEE/LEOS International Conference on Optical MEMS and their applications, 166-167 (2006).
31. P. J. Dwyer, C. A. DiMarzio, J. M. Zavislan, W. J. Fox, and M. Rajadhyaksha, "Confocal reflectance theta line scanning microscope for imaging human skin *in vivo*," Opt. Lett. **31**, 942-944 (2006).
32. T. Wilson and A. R. Carlini, "Size of the detector in confocal imaging systems," Opt. Lett. **12**, 227-229 (1987).
33. M. Gu, C. J. R. Sheppard, and X. Gan, "Image formation in a fiber-optical confocal scanning microscope," J. Opt. Soc. Am. A **8**, 1755-1761 (1991).
34. A. W. Snyder and J. D. Love, *Optical Waveguide Theory* (Chapman & Hall, London, 1983), Chap. 15.
35. R. H. Webb, "Confocal optical microscopy," Rep. Prog. Phys. **59**, 427-471 (1996).
36. K. B. Sung, C. Liang, M. Descour, T. Collier, M. Follen, A. Malpica, and R. Richards-Kortum, "Near real time *in vivo* fibre optic confocal microscopy: sub-cellular structure resolved," J. Microsc. **207**, 137-145 (2002).
37. W. M. White, M. Rajadhyaksha, S. Gonzalez, R. L. Fabian, and R. R. Anderson, "Non-invasive imaging of human oral mucosa *in vivo* by confocal reflectance microscopy," Laryngoscope **109**, 1709-1717 (1999).
38. A. L. Clark, A. M. Gillenwater, T. G. Collier, R. Alizadeh-Naderi, A. K. El-Naggar, and R. Richards Kortum, "Confocal microscopy for real-time detection of oral cavity neoplasia," Clin. Cancer Res. **9**, 4714-4721 (2003).
39. R. H. Webb, "Optics for laser rasters," Appl. Opt. **23**, 3680-3683 (1984).

1. Introduction

Confocal microscopy has become an established technique in many areas of experimental biology, enabling high-resolution imaging of cellular structure within a thin optical section [1]. The technique has been extended to enable confocal imaging *in vivo* [2], providing cellular-level resolution to depths of several hundred micrometers within living tissue. Initial clinical

#82105 - $15.00 USD Received 16 Apr 2007; revised 7 Jun 2007; accepted 8 Jun 2007; published 10 Jul 2007

applications in human subjects were focused in the ophthalmology [3] and dermatology [4] fields, where the tissue of interest is relatively accessible. Development of compact handheld probes enabled confocal microscopy to be applied to imaging the oral and cervical cavities, and several studies in these areas demonstrated the potential of the technique to identify characteristic neoplastic changes in morphology at the cellular level [5,6].

In order to translate the imaging capabilities of confocal microscopy to more confined spaces within the body, imaging probes have to be further reduced in size. Fiber-optic components and miniature optical elements are well suited to this task, but several technical challenges arise. To generate the confocal image, an optical beam must be focused and scanned across the sample at high speed, and this must take place at the distal (output) end of a probe measuring only a few millimeters in diameter.

Existing solutions to this problem include the use of tuning forks or piezoelectric actuators to physically deflect the tip of a single optical fiber [7-9] or to scan a fiber and objective lens together [10]. Alternatively, the scanning requirement can be reduced to one axis only by encoding the fast scan dimension in wavelength, and using a micromotor to sweep the resulting spectrum across the sample [11,12]. A means of mechanically scanning the beam at the distal end of a fiber can be eliminated altogether by the use of a fiber-optic bundle, comprising thousands of individual fibers drawn into a single element. The optical beam (either a point or line) can be scanned across the proximal (input) end of the bundle, generating a matching scan pattern at the distal end, which is imaged onto the tissue by a stationary objective lens [5,6,13-17]. Eliminating the need for a mechanical scanning element at the distal end of a probe can simplify efforts to miniaturize the device. However, drawbacks associated with the fiber bundle include the inherent pixilation artifact due to the finite spacing between individual fibers, and a limitation on the system's lateral resolution imposed by sampling requirements.

The recent development of miniaturized scanning mirrors based on microelectromechanical systems (MEMS) technology has enabled compact single-fiber imaging probes with distal scanning mechanisms to become feasible, eliminating the need for a fiber bundle while maintaining a small outer diameter [18-22]. Mirrors with sub-millimeter dimensions can be batch fabricated from a silicon-on-insulator (SOI) wafer, following multiple etching steps to leave a tilting mirror surface attached to the fixed substrate. A single gimbal-mounted surface capable of rotating about orthogonal axes can scan an optical beam over a two-dimensional raster pattern, eliminating the need to cascade successive one-dimensional scanners. Current MEMS scanning technology indicates that combdrive actuators are generally capable of scanning the mirror through larger angles, compared to parallel-plate actuators [23]. In order to fully utilize the size and performance features of the latest MEMS scanning devices in an optical imaging probe, the objective lens used to focus the scanning beam onto a sample must also be miniaturized. Previous work in reflectance confocal microscopy has relied on custom-designed lenses to provide a high numerical aperture in a small-diameter objective [17,24,25], though off-the-shelf elements only a few millimeters in diameter have become increasingly available at relatively low cost.

Researchers in confocal microscopy [19-22], optical coherence tomography [26,27] and multi-photon microscopy [28] have demonstrated prototype devices using MEMS scanners, with the goal of deploying these imaging technologies to sites within the human body. We previously demonstrated a MEMS-based confocal microscope, imaging cell phantoms and tissue specimens through a conventional microscope objective lens [21]. Here we present a confocal microscope using a single optical fiber, 0.5 mm x 0.5 mm scanning mirror, and a 5 mm diameter miniature objective lens. We provide details of the system design and performance, demonstrate its ability to resolve cellular structure in *ex vivo* and *in vivo* human tissues, and discuss practical design considerations specific to endoscopic confocal reflectance imaging in the clinical setting.

#82105 - $15.00 USD Received 16 Apr 2007; revised 7 Jun 2007; accepted 8 Jun 2007; published 10 Jul 2007

2. Methods

2.1 System details

A schematic diagram of the single-fiber confocal microscope (SFCM) system is shown in Fig.1(a). The light source is a fiber-coupled diode laser (Blue Sky Research) with a center wavelength of 635 nm and linearly-polarized output power of 25 mW. Light from the single-mode polarization-maintaining (PM) source fiber is collimated to a $1/e^2$ diameter of 1 mm, and aligned for transmission (*p*-polarized) through a bulk-optic polarizing beamsplitter (PBS1). This light is coupled into a second single-mode (PM) fiber for delivery to the sample stage. At the distal end of this PM fiber, light in the same (linearly-polarized) state emerges and is collimated to a diameter of 0.5 mm, before passing through a quarter-wave plate with its optic axis at 45° to that of the PM fiber.

The circularly-polarized beam is raster scanned in the plane normal to its direction of propagation by the MEMS scanner, comprising a 2-axis gimbal-mounted mirror (500 µm × 500 µm scanning area) with electrostatic vertical comb actuators. The device was fabricated by a series of deep reactive-ion etching stages of a two-layer SOI wafer [29]. The inner axis of the MEMS scanner is operated at its resonant frequency of 6.37 kHz, and the outer axis is actuated well below resonance, at a frequency of 8 Hz. Both axes are driven by sinusoidal waveforms, to minimize ringing in the response that was observed with triangular or sawtooth waveforms. The measured (total optical) angular deflections at near-maximum driving amplitudes were 11.3° and 5.5° for the fast and slow axes respectively.

The scanning mirror is positioned at the back focal plane of the miniature objective lens, with the objective-scanner-collimator combination designed to be telecentric on both fiber and tissue sides. Light returning from the sample is collected by the miniature objective, descanned at the MEMS device, and coupled back into the PM single-mode fiber. The quarter-wave plate rotates the polarization state of backscattered light through 90º relative to the incident light, resulting in light from the sample propagating back through the PM fiber along its orthogonal axis. On its return to PBS1, only light that has made a round-trip through the QWP will be reflected towards the detector (*s*-polarized), minimizing unwanted contributions from specular reflections in the optical path that remain *p*-polarized. A second polarizing beamsplitter (PBS2) oriented at 90° to PBS1 is used to further reduce the amplitude of unwanted reflections reaching a multimode fiber-connectorized avalanche photodiode (APD) with integrated amplifier module (Hamamatsu, C5460). The amplified APD signal and trigger signals synchronized with each axis' driving waveform are connected to a video frame grabber (Mu-Tech, MV-1000) for image reconstruction and continuous display.

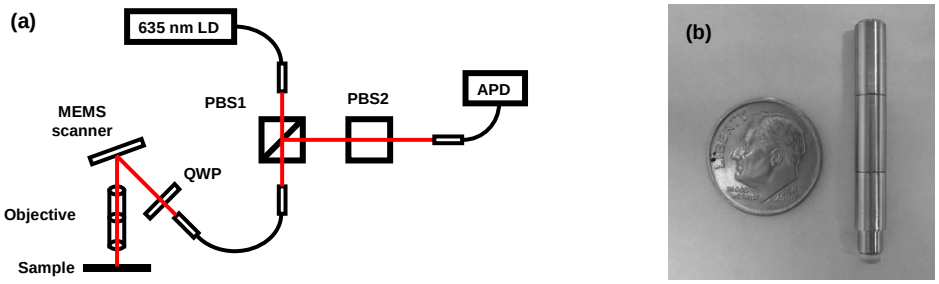

Fig. 1. (a) Schematic diagram of the single-fiber confocal microscope system. PBS: polarizing beamsplitter, QWP: quarter-wave plate, APD: avalanche photodiode. (b) Photograph of the miniature objective lens module alongside a US dime. The beam from the MEMS scanner enters at the bottom.

#82105 - $15.00 USD Received 16 Apr 2007; revised 7 Jun 2007; accepted 8 Jun 2007; published 10 Jul 2007

The miniature objective lens module is pictured in Fig. 1(b), and its optical layout presented in Fig. 2. The assembled module has a 5 mm outer diameter, is 35 mm in length, and is constructed from three commercial lens elements and a 300 μm thickness optical window (BK7). Each lens is 3 mm in diameter, with the first two achromatic elements (Edmund Optics, f_1 = 4.5 mm, f_2 = 12 mm) chosen to produce a magnified image (x 2.67) of the MEMS scanner at the back focal plane of the third lens (aspheric, Thorlabs, f_3 = 2 mm). With a collimated beam of 0.5 mm diameter incident on the miniature objective, the design NA at the object side is 0.33. Imaging is performed through a 0.3 mm thick BK7 glass window, under water immersion conditions (n = 1.33).

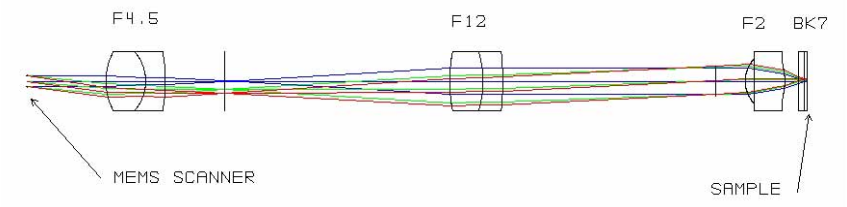

Fig. 2. Optical design of the miniature objective lens. Each lens is 3 mm in diameter, and the total distance between the scanner and sample plane is 39.3 mm.

The system delivers an optical power of 2.75 mW to the sample, with the most significant source of power loss (~ 5 dB) due to the low reflectivity of the uncoated MEMS scanner. While the current scanning surface is uncoated silicon (measured R ≈ 32% at 635 nm), techniques have recently been developed to add an additional metallic layer to the scanning surface, increasing the reflectivity to around 70-80% without adversely affecting scanner performance [18,30].

2.2 Tissue specimens

For *ex vivo* tissue imaging, human oral biopsy specimens were obtained from The University of Texas MD Anderson Cancer Center, Houston, TX, under a protocol approved by MD Anderson and Rice University. After embedding in agarose, specimens were sliced into 200-400 μm-thick transverse sections for confocal imaging. The use of transverse sections enabled us to image tissue features over the full specimen thickness without suffering from loss of signal at increased depths. While this arrangement is clearly not representative of *in vivo* imaging, it is an effective way to evaluate the SFCM's ability to distinguish the distinct features of the layered structure. Once SFCM imaging was complete, sections were immediately imaged on a Lucid Vivascope 2500 confocal reflectance microscope for comparison.

3. Results

3.1 Theoretical analysis of the miniature objective

Figure 3(a) shows the geometrical spot diagram for the miniature objective, determined by sequential ray tracing in ZEMAX® optical design software. The analysis propagates rays through the optical system from user-specified locations (or "fields") on the object or image planes, as shown in Fig. 2, where three rays (of matching color) are traced from each of three fields. The spot diagram presents the pattern of rays at the image (sample) plane of the objective, for the three image fields at 0 μm (on-axis, blue rays), 100 μm (at one edge of the full FOV, red rays), and 70.7 μm ($\sqrt{2}$ FOV, green rays). The most significant aberration is field distortion, but the propagated rays remain within the Airy disk (shown as a black circle in Fig. 3(a) for all positions except a few rays at the edge of the full FOV. The calculated root-mean-squared spot diameter is 0.148 μm on axis, and 1.248 μm at the edge of the fields.

#82105 - $15.00 USD Received 16 Apr 2007; revised 7 Jun 2007; accepted 8 Jun 2007; published 10 Jul 2007

The Airy disk is 2.3 μm in diameter, indicating that the objective is expected to provide diffraction-limited performance over almost the full FOV. The modulation transfer function for each of the three field positions shown in (a) is plotted in Fig. 3(b), alongside the diffraction-limited MTF. The tangential (T) and sagittal (S) responses are shown for each field point, in colors corresponding to Fig. 3(a). By this measure, the objective's performance is also predicted to be close to the diffraction limit, with the largest deviation again predicted at field positions near the edge of the 200 μm field-of-view.

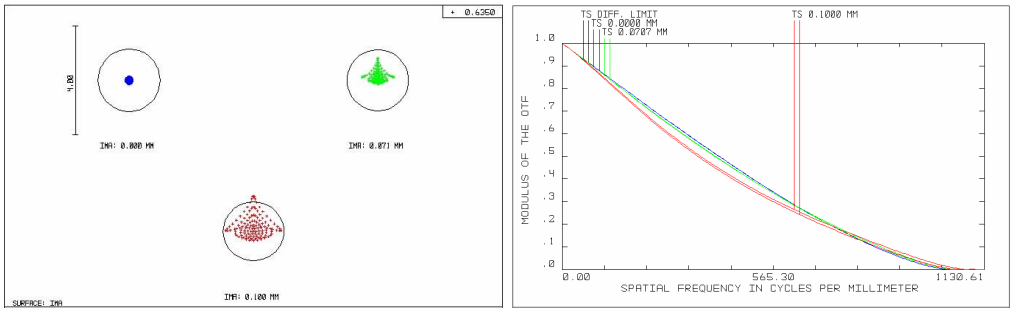

Fig. 3. Spot diagram (a) and modulation transfer function (b) computed for the three-element miniature objective. The plots shown in (b) correspond to the three field positions indicated in (a), alongside the diffraction-limited case.

The working distance of the miniature objective can be adjusted by changing the separation between the third lens element and the optical window. All images presented here were taken with a working distance of approximately 150 μm, and as for a conventional confocal microscope, this parameter ultimately limits the axial imaging range.

3.2 Imaging performance

The axial resolution was determined by recording the power level at the detector while moving a plane mirror surface through the objective's focal plane, with the MEMS scanner held stationary. Figure 4(a) shows the measured intensity profile, with a full-width at half maximum (FWHM) of 9.55 μm. The lateral resolution was determined by translating a reflective edge across the focal plane, yielding a 90%-10% intensity transition over a distance of 0.83 μm (Fig. 4(b)), corresponding to a FWHM of 0.78 μm assuming a Gaussian spot [2,31]. The resolution of the confocal microscope depends on the sizes of the illumination source and the detector, and many researchers account for the effect of using a finite-sized pinhole by following the analysis of Wilson and Carlini [32]. The fiber-optic confocal microscope requires a slightly different treatment, since the optical fiber acts as both a finite-sized source *and* detector, and the measured signal level is dependent on field amplitude at the fiber, rather than intensity at a pinhole. We applied the analytical results of Gu *et al* [33] to our system, using the manufacturer's specifications to determine the "fiber spot size" [34] and corresponding fiber parameter. The FWHM of the detected intensity profile as a perfectly-reflecting planar object is translated through focus is expected to be 7.14 optical units, or 8.81 μm in our system. The corresponding analysis of lateral resolution by Gu *et al* is limited to determination of the coherent transfer functions for a point object, and does not extend to analytical expressions for the intensity point-spread function. We therefore returned to Wilson and Carlini [32] and treated the fiber as a pinhole with a size given by its mode-field diameter (4.5 μm). Although this analysis neglects the finite size of the illumination source, and treats the light-collecting properties of the fiber as identical to a pinhole, we proceeded nevertheless and determined a theoretical lateral resolution of 2.52 optical units, or 0.77 μm (FWHM).

#82105 - $15.00 USD Received 16 Apr 2007; revised 7 Jun 2007; accepted 8 Jun 2007; published 10 Jul 2007

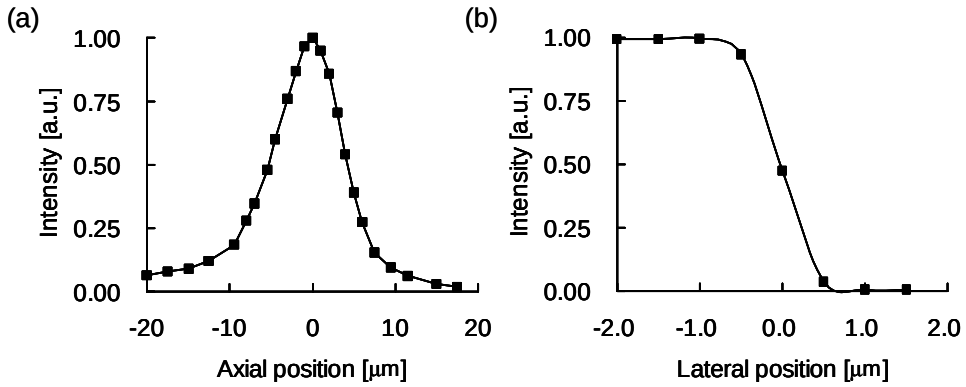

Fig. 4. Axial and lateral resolution measurements. (a) Normalized intensity measured as a mirror was translated axially through the focus, FWHM = 9.55 μm. (b) Normalized intensity measured as a reflective edge was translated laterally across the focus, 90%-10% transition = 0.83 μm.

The measured resolution values in both axial and lateral directions were in good agreement with theoretical values, which assume uniform illumination of the objective lens. We chose to slightly sacrifice resolution in favor of increased throughput by matching the $1/e^2$ width of the Gaussian beam to the objective aperture [35]. An image of the group 7 elements in a positive USAF resolution target is shown in Fig. 5. The smallest lines in the group are 2.19 μm wide and clearly resolved, and the field-of-view is 140 μm x 70 μm.

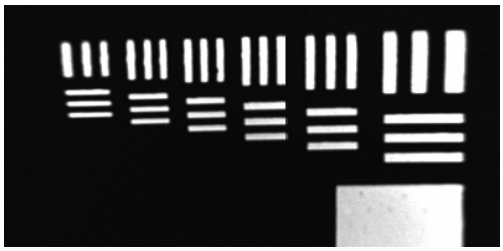

Fig. 5. Reflectance image of a USAF resolution target, group 7 elements 1-6, acquired with the MEMS confocal microscope. The field-of-view is 140 μm x 70 μm and the smallest bars are 2.19 μm wide.

3.3 Ex vivo tissue imaging

Figure 6 presents images from a tissue section that was clinically-normal in appearance, following application of 6% acetic acid solution to enhance nuclear contrast [36]. Soft oral mucosa is covered with a surface epithelium, comprised of layers of cells at different stages of differentiation. The basement membrane separates the epithelial layer from underlying connective tissue at a depth of approximately 200-500 μm. Many precancerous lesions originate in the epithelial layer, placing them within the range of confocal imaging. Figure 6(a) contains a sequence of images acquired at 8 frames-per-second (fps) with the SFCM device, compiled as a movie sequence that is representative of the real-time screen display during imaging. As the movie plays, the specimen is axially and laterally translated and several cells move through the field-of-view, with the strongly scattering nuclei exhibiting an elliptical appearance. Figure 6(b) presents an image of the same tissue slice, acquired with the Lucid confocal microscope at the same scale as the SFCM image in Fig. 6(a). Again, cell nuclei appear elliptical in shape, and more strongly scattering than their surroundings.

#82105 - $15.00 USD Received 16 Apr 2007; revised 7 Jun 2007; accepted 8 Jun 2007; published 10 Jul 2007

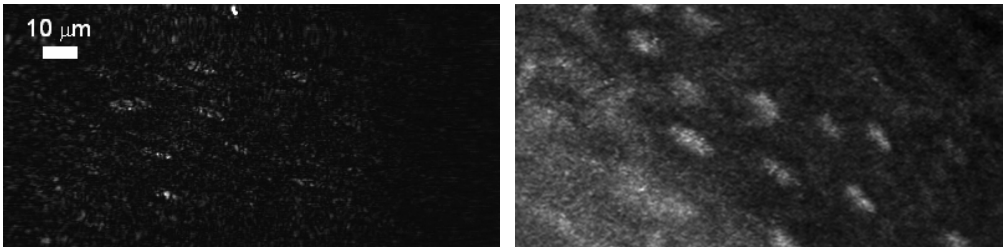

Fig. 6. Confocal reflectance images of *ex vivo* human oral tissue, (left) acquired with the MEMS confocal microscope and miniature objective. (Movie size 2.5 MB, 3 seconds at 8 fps). (Right) Image of the same tissue slice, acquired with the Lucid Vivascope 2500 confocal microscope.

3.4 In vivo tissue imaging

We imaged normal human oral mucosa from the lower lip of a volunteer, following application of 6% acetic acid solution. In Fig. 7(a), a sequence of images acquired with the SFCM at 8 frames per second is presented, with the confocal section now oriented parallel to the tissue surface, orthogonal to the transverse sections of Fig. 6. The field-of-view matches that of Figures 5 and 6 (140 μm x 70 μm), and cell nuclei approximately 10-15 μm in diameter can be seen, providing a stronger signal than their surroundings. As the movie plays, relative motion between the miniature objective's glass window and the tissue is evident in both axial and lateral directions, though several cells are retained within the field-of-view over the course of the 3-second movie. Effects due to motion artifacts are further demonstrated in an extended version of this image acquisition, during 15 seconds of continuous imaging. Again, individual cells can be maintained within the field-of-view for several seconds, even without any means of active tissue stabilization. An image of the lip of the same volunteer was acquired with the Lucid Vivascope 1500, shown in Fig. 7(b) at the same scale. Nuclei can again be identified as strong scattering centers relative to the cytoplasm [37,38] and cell membranes are also barely visible.

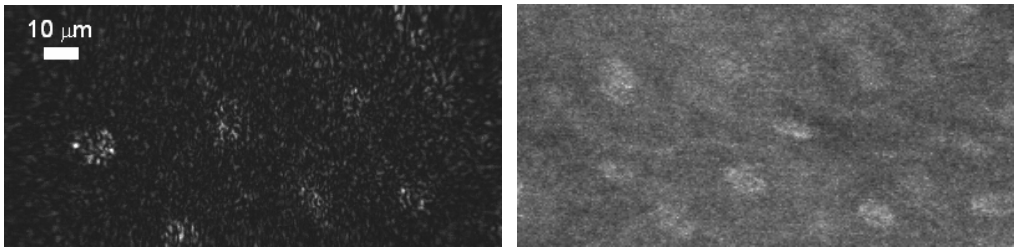

Fig. 7. (a) Images of normal *in vivo* human oral mucosa acquired with the MEMS confocal microscope and miniature objective. (Movie size 2.5 MB, 3 seconds at 8 fps. (9.6 MB version, 15 seconds at 8 fps). (b) Image of the same tissue from the same volunteer, acquired with the Lucid Vivascope 1500 confocal microscope.

4. Discussion

The aim of this project is to develop an imaging device to translate the established capabilities of *in vivo* reflectance confocal microscopy to sites within the body. MEMS scanners combined with single-mode fiber optics and miniature lens elements can avoid the drawbacks of fiber bundle-based imaging, and the overall package size can be kept small. This study was carried out to establish the feasibility and technical requirements of MEMS-based clinical imaging of the human oral cavity, *in vivo*.

To assist in our evaluation of images acquired with the SFCM device, each site (for both *ex vivo* and *in vivo* tissues) was imaged with an established, commercially-available system.

#82105 - $15.00 USD Received 16 Apr 2007; revised 7 Jun 2007; accepted 8 Jun 2007; published 10 Jul 2007

These systems operate with quite different imaging parameters; when compared to the SFCM, the Lucid system delivers approximately 3.6 times more power to the sample, operates at twice the duty-cycle, and is expected to achieve at least three times higher optical efficiency in the return path (mostly attributed to the likely difference in scanner reflectivity). These differences are approximately offset by the significantly larger field-of-view covered by the commercial system (0.25 mm^2 versus 0.01 mm^2 for the SFCM, a factor of 25). The operating wavelengths also differ (635 nm versus 830 nm), but it is the objective numerical aperture, with its linear effect on lateral resolution and quadratic effect in the axial direction, that is expected to have a significant effect on confocal image quality. The Lucid system NA is 0.9, compared to 0.33 for the SFCM, both under water immersion conditions.

Rajadhyaksha *et al* [2] qualitatively and quantitatively determined that the optimum NA for reflectance confocal microscopy of unstained, living skin lies in the range 0.7 – 1.2. If the optical section thickness (axial resolution) approaches the scattering mean-free path in tissue (typically 20-100 μm), then increasing numbers of multiply-scattered photons will be collected, adversely affecting image contrast. Although the axial resolution of the SFCM system was predicted and measured to be below 10 μm, this corresponds to the ideal case of a sample comprising a single planar reflecting surface. In a scattering medium such as tissue, the optical section thickness will be degraded relative to this optimum value due to scattering and aberrations, and we expect that our design will benefit from an increased NA to improve the rejection of multiply-scattered light. However, raising the NA of an objective while maintaining a small outer diameter is technically challenging, requiring high-power lenses with tight tolerances. A recently-presented approach addresses these issues by combining off-the-shelf glass and custom plastic lenses, with a miniaturized, self-centering mounting mechanism to achieve highly accurate lens positioning [25].

While this work has demonstrated that miniaturization of scanners and optical elements can result in a system with cellular imaging capability, an optimized design requires consideration of the distinct, but related concepts of *resolution*, and *resolvable points*. At any particular wavelength, the number of resolvable points in a scanning laser system is established by the scanner alone, determined by the product of its optical scan angle and aperture [39,28]. The objective lens serves only to relay these points to the object plane, with any magnification affecting NA (resolution) and field-of-view with the same linear dependence. In other words, any improvement in lateral resolution achieved by an increase in NA will be accompanied by a reduction in FOV by the same factor; the number of resolvable points is conserved. Once the maximum size of the scanner is set by the constraints of an application, the only way to further increase the number of resolvable points is to increase its scan angle. The role of the optics is to balance the trade-off between resolution and field-of-view, while working within any additional constraints on device diameter and working distance.

Imaging tissue *in vivo* with MEMS-based confocal microscopes is challenging, and in order to reproducibly acquire images during routine clinical use, further development will be necessary. Minimizing subject and operator motion will be a critical factor, though these effects can be addressed through active tissue stabilization, and mitigated by an increase in the image field-of-view. Miniaturized objective lenses with integrated hydraulic lines have been designed and tested for confocal imaging [25], with the sample held in place against the objective by gentle suction. As described above, an increased field-of-view can only be achieved through modifications to the scanner performance, if resolution is to be preserved. Recent MEMS scanners based on a similar design to those used in this work have been demonstrated for two-photon imaging [28], with a 750 μm aperture. This 50% increase relative to our 500 μm-sized scanners can be translated into a proportionate increase in either field-of-view or NA. The 70 μm scan range achieved here along the slow axis was under a single-sided driving voltage only, and a doubling of this axis' range is expected if the scanner is driven on both sides of its zero position.

#82105 - $15.00 USD Received 16 Apr 2007; revised 7 Jun 2007; accepted 8 Jun 2007; published 10 Jul 2007

5. Conclusions

Since the first demonstrations of MEMS-based confocal microscopy in the early 1990's, the optical and mechanical performance of miniaturized scanning devices has matured to the stage where their use in *in vivo* endoscopy has become feasible. When used in combination with fiber-optic components and miniaturized objective lenses, MEMS-based confocal microscopes can provide images at cellular resolution in living subjects. Future studies will evaluate the capability of this system to assist clinicians in oral cancer diagnosis.

Acknowledgments

Financial support from the National Institutes of Health is gratefully acknowledged (grants R01 CA82880 and R01 CA103830). This work was also supported by a Korea Research Foundation Grant funded by the Korean Government (MOEHRD, Basic Research Promotion Fund, KRF-2005-214-C00058).

#82105 - $15.00 USD Received 16 Apr 2007; revised 7 Jun 2007; accepted 8 Jun 2007; published 10 Jul 2007